Effect of a longitudinal crack on the flexural performance of bamboo culms

Theodora Mouka[1], Elias G. Dimitrakopoulos[1*] and Rodolfo Lorenzo[2]

[1]Department of Civil and Environmental Engineering, The Hong Kong University of Science and Technology, Clear Water Bay, Kowloon, Hong Kong, China.
[2]Department of Civil, Environmental and Geomatic Engineering, University College London, Gower Street, London, WC1E 6BT, UK.

*Corresponding author(s). E-mail(s): ilias@ust.hk;
Contributing authors: tmouka@connect.ust.hk; r.lorenzo@ucl.ac.uk;

Abstract

Splitting parallel to the culm fibers is common in full-culm bamboo structural members, even early in a structure's lifespan. Currently, there is insufficient knowledge on the effect of splitting on member performance, which induces significant uncertainties in bamboo member engineering design. This is a potential threat to the safety of existing and future full-culm bamboo structures. This study investigates analytically the effect of a longitudinal crack on the stiffness of an originally intact bamboo culm in flexure. The study develops analytical expressions that describe stiffness loss in two flexure cases (a three-point bending and a four-point bending test), and verifies them with available experimental results and numerical simulations. Main cause of the stiffness loss are torsion-induced deflections, with secondary cause being shear deformations. Importantly, stiffness loss solely depends on two dimensionless parameters: shape factor (radius-to-thickness ratio), and a factor that is a function of material properties and ratio of shear span length to culm diameter. Additionally, the study proves analytically that friction at the load application points mitigates torsion-induced deflections. This has important implications for bamboo structure design and testing standards, indicating that the manner in which loads are transferred on beams affects the apparent beam stiffness when a crack appears.

Keywords: Full-culm bamboo bending, Stiffness loss, Vlasov torsion, Warping, Longitudinal crack

1 Introduction

Bamboo as a structural material has incited the interest of researchers in recent decades, because of its high strength-to-weight ratio [1], fast growth [2, 3] and low carbon footprint [4]. These traits render bamboo a promising alternative to conventional construction materials, whose production generates the majority of the construction industry carbon emissions [5]. However, an obstacle to widespread utilization of bamboo in construction is the scarcity of detailed design and testing standards (notwithstanding recent advances [6]), and the currently incomplete comprehension of bamboo structural member behavior.

The complexity of bamboo structural member behavior partly stems from bamboo culm morphology, which comprises longitudinal fibers encased in a lignin matrix, much akin to a uni-directional fiber-reinforced composite [3, 7–9]. This leads to low tensile strength perpendicular to the fibers, and hence bamboo is prone to splitting parallel to the fibers [10–13]. Splitting can even occur during the process of bamboo culm drying, or because of ambient humidity variations [14]. This is because moisture variations within the culm cause volumetric changes. The moisture variations (and thus the volumetric changes) are not uniform within the culm wall, because of the density variation along the culm thickness. This in turn leads to volumetric change restraints, and therefore to additional stresses (that do not stem from external loads). When these stresses exceed the low circumferential tensile strength of bamboo, longitudinal cracks appear. Thus, longitudinal cracks during the lifespan of a bamboo structure are common, and therefore a better understanding of the behavior of cracked bamboo structural members is crucial for the design of bamboo structures.

Research on bamboo splitting has mainly focused on the stress at crack initiation, and the mechanisms that cause splitting [10–12, 15]. Other studies have investigated bamboo fracture properties, which pertain to crack propagation [16–19]. Hence, there is little knowledge on the implications of splitting, and on member behavior after the appearance of cracks, and it mainly comes from very recent (2022) studies [13, 20]. These studies indicate that, especially in full-culm bamboo flexural members, longitudinal cracks lead to significant stiffness loss, which starts notably earlier than eventual failure [12]. Further, a recent (2022) experimental study [20] proved that, when there is a single longitudinal crack at the side of a bamboo culm, its bending stiffness during a three-point bending test can drop by 40%∼65%, because of torsional effects.

In general, given the ubiquity of bending tests in characterizing flexural members in structural engineering (e.g., in design codes and testing standards), there is a need to characterize the bending stiffness of a slit culm. In this context, the opening of a single crack at the side of a full-culm flexural member alters the problem mechanics significantly, because the culm cross-section transitions from a closed section to an open section. This has important implications on the shear flow within the cross-section, and thus on the shear-induced deflections. Additionally, the cross-section shear center shifts, inducing torsional effects, and hence additional torsion-induced deflections [21]. This study considers a single crack at the mid-height of the culm, as this is where cracks usually appear in bamboo culms subjected to bending, because of the high shear and circumferential tensile stresses in that location [12, 13, 15]. A crack at the mid-height of the culm is critical, because it maximizes the eccentricity of the applied transverse loads, with respect to the shear center, which in turn maximizes the applied torque on the culm. The simultaneous presence of warping, because of the open cross-section shape [22], further complicates the problem.

The present study examines the shear- and torsion-induced stiffness loss of slit bamboo culms, complementing the recent study of the authors [13], which did not account for these effects. More specifically, the study investigates analytically stiffness loss in two cases of flexure; a three-point bending and a four-point bending test. As a verification, the study compares the analytical predictions to pertinent experimental results [20] and numerical simulations. The motivation is to complement current knowledge on the behavior of full-culm bamboo flexural members, and thus to alleviate the uncertainties the occurrence of cracking imposes on their safe engineering design.

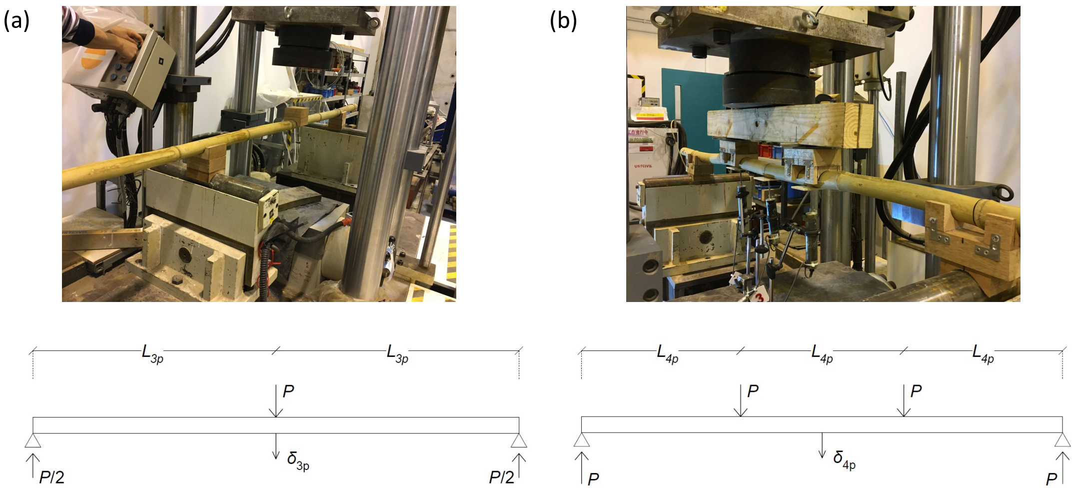

Fig. 1 (a) Three-point bending test and (b) four-point bending test on bamboo.

2 Effect of shear

When a crack appears at the side of an initially intact culm, the culm cross-section transitions from a closed section to an open section. This alters the shear flow in the cross-section, and thus the shear correction factor, which comes into the shear-induced deflection calculations [23]. This section examines analytically the contribution of shear deformations on the total deflection at the midspan, before (closed section) and after (open section) a crack appears at the side of a bamboo culm. All the calculated deformations occur via the virtual work method, and assume that the stress-strain equations are according to the transversely isotropic stiffness tensor. In this context, the equations ignore any higher-order deformations, e.g., because of local effects (local loads, support conditions, etc.), which can be important in highly anisotropic materials [24, 25]. Moreover, in the open section case, the analysis assumes that the crack is present along the entire span length, and therefore it is a lower-bound approach for the stiffness calculations. All the calculations assume thin-walled sections for simplicity, and thus their accuracy is expected to be reduced for thick-walled section cases. The analysis considers two cases: three-point flexure (fig. 1a), and four-point flexure according to [26] (fig. 1b). Note that, in the reference four-point bending test, the distance between the applied loads is equal to the shear span (fig. 1b), which is a typical test setup for bamboo culms [12, 15, 27].

The first step is to determine whether shear-induced deflections are significant with respect to deflections due to the bending moment. The deflection δ_b at the midspan because of the bending moment is the same for closed and open sections. For a three-point bending test:

$$\delta_{b,3p} = \frac{PL_{3p}^3}{6E_{\parallel}I} \tag{1}$$

where P is the load at the midspan, $E_{\parallel}$ the Young's modulus parallel to the fibers [25], and I the cross-section moment of inertia ($I = \pi R^3 t$ for a thin-walled cylinder, where R is the midline radius and t the thickness). L_{3p} denotes the shear span length of the three-point bending test, equal to 1/2 of the total span length (fig. 1a). Respectively, for the four-point bending test of fig. 1b:

$$\delta_{b,4p} = \frac{23PL_{4p}^3}{24E_{\parallel}I} \tag{2}$$

where P is half of the total load and L_{4p} the shear span length, equal to 1/3 of the total span length (fig. 1b). The deflections because of shear for the three-point ($\delta_{s,3p}$) and the four-point ($\delta_{s,4p}$) bending tests are:

$$\delta_{s,3p} = \frac{PL_{3p}}{2k_s G_{\parallel} A} \tag{3}$$

$$\delta_{s,4p} = \frac{PL_{4p}}{k_s G_{\parallel} A} \tag{4}$$

where k_s is the shear correction factor (which depends on the cross-section shape), $G_{\parallel}$ is the shear modulus parallel to the fibers [25], and $A = 2\pi Rt$ the cross-section area. For a thin-walled cylinder, k_s is 0.5 for a closed section [23] and approximately 0.17 for an open section [28], when the crack is at the side.

Equations 1 and 3, and eqs. 2 and 4 give:

$$\frac{\delta_s}{\delta_b} = \frac{3\Theta}{c_i k_s} \tag{5}$$

where $c_i = 8$ for the three-point bending test and $c_i = 23$ for the four-point bending test. Θ is a dimensionless parameter we introduce herein (namely, shear-torsion deflection factor, see also Section 3), and depends on material properties and on the dimensionless shear span length $n = L/(2R)$ (where L is the shear span length and $D = 2R$ the culm midline diameter):

$$\Theta = \frac{E_{\parallel}}{n^2 G_{\parallel}} \tag{6}$$

For the same shear span length (therefore, for the same shear deflections), the ratio of shear deflection over bending deflection is 2.9 times higher in the three-point bending test compared to the four-point bending test (which, as expected, is the ratio of the bending deflections of the two load cases).

Figure 2 plots eq. 5 for typical for bamboo $E_{\parallel}/G_{\parallel}$ ratios, and for the cases of open and closed section. In fig. 2b, ratio δ_s/δ_b is larger than 1 for high values of $E_{\parallel}/G_{\parallel}$, therefore, in these (extreme) cases, shear deflection has larger contribution to the total deflection than the deflection because of the bending moment. Figure 3 illustrates the effect of the shear-torsion deflection factor Θ (eq. 6) on the shear-induced deflections (eq. 5). As expected, a low Θ (corresponding to high shear modulus $G_{\parallel}$, with respect to the longitudinal Young's modulus $E_{\parallel}$, or to a long shear span length) leads to considerable mitigation of shear-induced deflections. Interestingly, for a fixed Θ value, the ratio of shear over bending deflection is the same for an open-section four-point bending test and a closed-section three-point bending test (fig. 3). This is likely coincidental, as the product $c_i k_s$ is the same for the two cases.

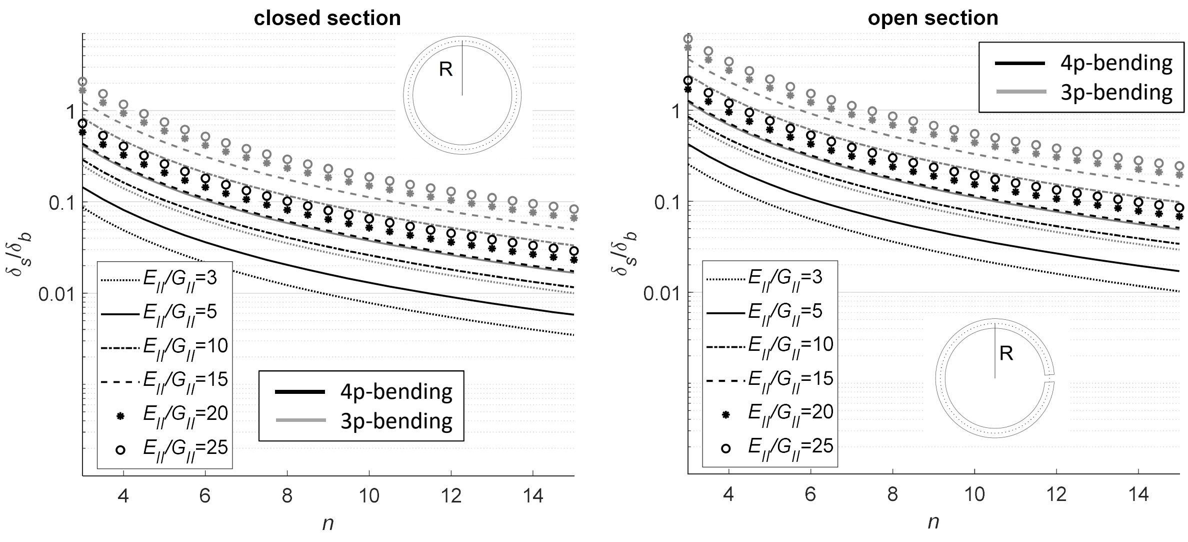

Fig. 2 Contribution of shear to the deflection at the midspan versus normalized shear span length ($n = L/(2R)$, for various $E_\parallel/G_\parallel$ ratios ($E_\parallel$ is the longitudinal Young's modulus and $G_\parallel$ the shear modulus parallel to the fibers).

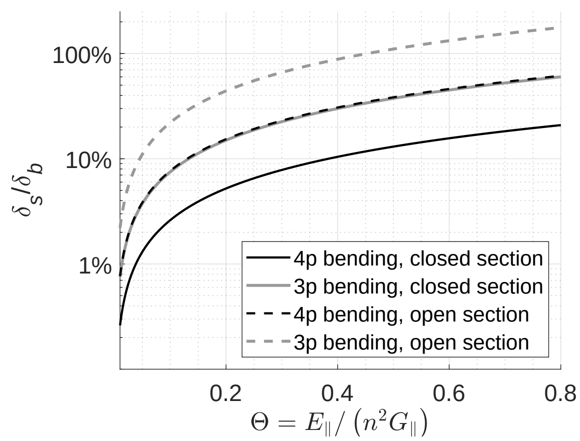

Fig. 3 Contribution of shear to the deflection at the midspan versus shear-torsion deflection factor $\Theta = E_\parallel/(n^2 G_\parallel)$.

As an example, consider a Moso bamboo culm (*Phyllostachys edulis*) subjected to bending. Reported average material properties are $E_\parallel$=12500∼20000 MPa (e.g., [12, 20, 29]) and $G_\parallel$=2830 MPa [29], therefore $E_\parallel/G_\parallel$ ≈4.5-7.0. Hence, in a closed-section four-point bending test, shear deformations are negligible (less than 2% δ_b) for shear span lengths larger than approximately 8 times the culm diameter (fig. 2). In contrast, in three-point bending, shear deformations are negligible only for very large shear span lengths (n >12) in the closed section case (fig. 2 left). In the case of slit culms (open section), shear deformations cannot be ignored in most of the cases (for both tests, fig. 2 right).

3 Effect of torsion

3.1 Torsion problem description

When a crack appears, the cross-section transitions from closed to open section. An important consequence of that is the translation of the shear center. Specifically, the shear center of the cross-section moves from the center of the tube (point O) to point S, at a distance of one diameter from point O, opposite the crack location (fig. A1a). To get a better understanding on how that affects the apparent stiffness, consider a crack at the side of the culm, (fig. A1a) along the entire culm length. This is the crack position that maximizes the applied torque, and therefore it is a lower-bound approach for the stiffness calculations. Once the crack opens, load P does not pass through the shear center, and therefore it creates a torque T_0 (fig.A1b,c), of magnitude $2PR$. The work of the newly-induced torsional load creates additional deflections, that contribute to an apparent stiffness loss. This section calculates the torsion-induced deflections at the middle of the culm for the four-point bending test. The corresponding calculations for the three-point bending test can be found in Appendix B. Note that the herein presented calculations ignore the (imperfect) warping restraint the nodes induce. Taking that into account, would lead to smaller deflections; however, deriving the pertinent equations is a complicated task, beyond the scope of this study.

Determining the pertinent deflections requires solving the torsion problem at hand, which is a Vlasov torsion-warping problem [22]. Hence, part of the torque is resisted by Saint-Venant shear stresses, and part of it by shear stresses, induced because of warping. Let T_s be the Saint-Venant torque and T_w the warping torque. It follows that, at every point along the culm:

$$T_s + T_w = T_{tot} \tag{7}$$

where T_{tot} is the total torque. Integrating eq. 7 along the culm length:

$$B_s + B_w = B_{tot} \tag{8}$$

where B is the bimoment:

$$B = -\int T dz \tag{9}$$

In eq. 9, T denotes the torque and z the longitudinal direction of the culm (fig. A2). Of specific interest are Saint-Venant torque T_s and warping bimoment B_w (eqs. 7 and 8), as these are the forces that produce work, and therefore contribute to the deflections associated with torsion. T_s and B_w relate to the angle of twist θ as:

$$T_s\left(z\right) = G_{\parallel} J_s \theta'\left(z\right) \tag{10}$$

$$B_w\left(z\right) = E_{\parallel} J_w \theta''\left(z\right) \tag{11}$$

where $G_{\parallel}$ is the shear modulus parallel to the fibers [30], J_s is the torsional constant and J_w the sectorial moment of inertia (warping constant). In the case of a thin-walled open tube [23]:

$$J_s = \frac{2}{3}\pi R t^3 \tag{12}$$

$$J_w = \frac{2}{3}\left(\pi^3 - 6\pi\right) R^5 t \tag{13}$$

where R is the midline radius and t the thickness.

Therefore, to determine the deflections associated with torsion, we need to determine the angle of twist θ along the culm. To that end, θ occurs by solving the differential equation:

$$E_{\|} J_w \theta'''' (z) - G_{\|} J_s \theta'' (z) = m_z (z) \tag{14}$$

where $m_z(z)$ is the distributed torque along the member. On the left-hand side of eq. 14, the first term corresponds to warping and the second term to Saint-Venant torsion. Considering that, in the bending tests under consideration, $m_z(z)$=0, the solution of eq. 14 is:

$$\frac{B_w (0)}{\lambda^2} \cosh(\lambda z) - \frac{T_w (0)}{\lambda^3} \sinh(\lambda z) + \alpha_1 z + \alpha_2 = E_{\|} J_w \theta (z) \tag{15}$$

where $B_w(0)$ and $T_w(0)$ are the warping bimoment and the warping torque at z=0 (fig. A2), α_1 and α_2 are integration constants, and λ is:

$$\lambda = \sqrt{\frac{G_{\|} J_s}{E_{\|} J_w}} \tag{16}$$

To determine θ along the culm, this study takes advantage of symmetry, considering only half of the culm (fig. A2). It also assumes, as a first approximation, that the culm does not twist at the support (end i), and that the test setup at the load application points does not constrain twisting. This means that, at the support (end i), the member is free to warp (θ_i''=0) but does not twist (θ_i=0) and at the middle (end k) it is free to twist (T_k=0 if there is no applied torque at that point) but does not warp (θ_k'=0) (fig. A2), because of symmetry of the warping deformations.

After solving the torsion problem, the deflection δ_t (at the middle of the culm), associated with torsion, occurs from the virtual work method as:

$$\delta_t = 2 \int_0^{z_m} \frac{T_s \overline{T}_s}{G_{\|} J_s} dz + 2 \int_0^{z_m} \frac{B_w \overline{B}_w}{E_{\|} J_w} dz \tag{17}$$

where z_m is $1.5L_{4p}$ for the four-point bending test and L_{3p} for the three-point bending test (fig. A2). $\overline{T}_s$ and $\overline{B}_w$ are the Saint-Venant torque and warping bimoment for half of the unit load (because of symmetry) at the middle of the culm (end k, fig. A2a). Applying the boundary conditions, the following section calculates the unknown constants of eq. 15, and subsequently determines δ_t for the the four-point bending test. Appendix B provides similar calculations for the three-point bending test (which is a simpler case).

3.2 Torsion in the four-point bending test

For the four-point bending test, this study divides the (half) culm into two members, member (1) being from the support (end i) to the load (end j) and member (2) from the load (end j) to the middle of the culm (end k, fig. A2b). Then, it considers eq. 15 twice (once for each member), and specifies the unknowns $B_w(0)$, $T_w(0)$, α_1 and α_2 for each member, taking into account the boundary conditions at ends i, j and k (fig. A2b and Section 3.1). At end k, the torque is T_k=0 and, at end i, from equilibrium, $T_i = T_0$, where T_i is the torque reaction at the support, and $T_0 = 2PR$ is the applied torque at the load application point. The rest of the boundary conditions (at end j) occur from continuity requirements: $\theta_{1j} = \theta_{2j}$, $\theta'_{1j} = \theta'_{2j}$, $\theta''_{1j} = \theta''_{2j}$ (subscripts 1 and 2 denote members (1) and (2) respectively, fig. A2b). The resulting equation for the angle of twist θ_{4p} along the culm is:

$$E_{\parallel} J_w \theta_{4p}(z) = \begin{cases} \frac{2PR}{\lambda^2}\left\{z - \frac{\sinh(\lambda z)}{\lambda[2\cosh(\lambda L_{4p})-1]}\right\}, & 0 \le z \le L_{4p} \\ \frac{2PR}{\lambda^2}\left\{L_{4p} + \frac{\sinh(\lambda L_{4p})}{\lambda}\left[\tanh\left(\frac{3\lambda L_{4p}}{2}\right)\sinh(\lambda z) - \cosh(\lambda z)\right]\right\}, & L_{4p} \le z \le 1.5L_{4p} \end{cases} \tag{18}$$

where L_{4p} is the shear span length of the four-point bending test. Note that eq. 18 assumes that the culm does not twist at the supports.

Subsequently, substituting eq. 18 into eqs. 10 and 11, Saint-Venant torque $T_{s,4p}$ and warping bimoment $B_{w,4p}$ are:

$$T_{s,4p}(z) = \begin{cases} 2PR\left[1 - \frac{\cosh(\lambda z)}{2\cosh(\lambda L_{4p})-1}\right], & 0 \le z \le L_{4p} \\ 2PR\sinh(\lambda L_{4p})\left[\tanh\left(\frac{3\lambda L_{4p}}{2}\right)\cosh(\lambda z) - \sinh(\lambda z)\right], & L_{4p} \le z \le 1.5L_{4p} \end{cases} \tag{19}$$

$$B_{w,4p}(z) = \begin{cases} -2PR\frac{\sinh(\lambda z)}{\lambda[2\cosh(\lambda L_{4p})-1]}, & 0 \le z \le L_{4p} \\ 2PR\frac{\sinh(\lambda L_{4p})}{\lambda}\left[\tanh\left(\frac{3\lambda L_{4p}}{2}\right)\sinh(\lambda z) - \cosh(\lambda z)\right], & L_{4p} \le z \le 1.5L_{4p} \end{cases} \tag{20}$$

Equations 19 and 20 are valid, regardless of whether the culm twists at the supports, as long as the rest of the boundary conditions do not change. Further, utilizing the virtual work method (for more details, see Appendix B), the torsion-induced deflection at the midspan $\delta_{t,4p}$ for the four-point bending test is:

$$\delta_{t,4p} = \frac{12Pn\phi^3}{\pi G_{\parallel} R}\left\{1 - \frac{2\sinh\left(\frac{\lambda L_{4p}}{2}\right)}{\lambda L_{4p}\left[2\cosh(\lambda L_{4p}) - 1\right]}\right\} \tag{21}$$

where n is the normalized with culm diameter shear span length ($n = L_{4p}/(2R)$) and ϕ is the dimensionless shape factor of the culm, equal to the ratio of culm midline radius to thickness:

$$\phi = \frac{R}{t} \tag{22}$$

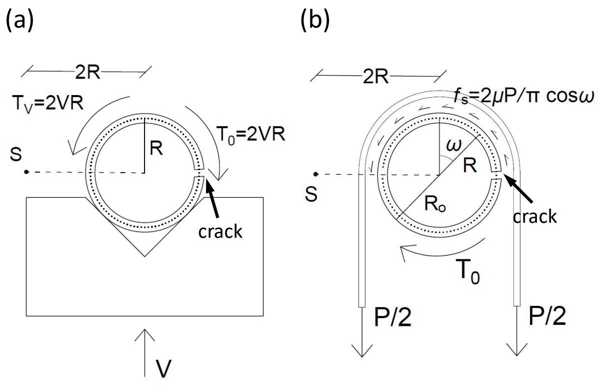

Fig. 4 a) Support: Torque induced by the support reaction and b)-d) Load application points: Effect of friction on the torque applied on the culm for various load application conditions: b) strap c) saddle and d) flat surface (e.g., steel plate)

Shape factor ϕ relates to the more commonly used for bamboo ratio of external diameter D_o to thickness t as:

$$\frac{D_o}{t} = 2\phi + 1 \tag{23}$$

Subsequently, combining eq. 21 with eq. 2:

$$\frac{\delta_{t,4p}}{\delta_{b,4p}} = \frac{36}{23}\Theta\phi^2 \left\{ 1 - \frac{2\sinh\left(\frac{\lambda L_{4p}}{2}\right)}{\lambda L_{4p}\left[2\cosh\left(\lambda L_{4p}\right) - 1\right]} \right\} \tag{24}$$

where Θ is the shear-torsion deflection factor, as in eq. 6. The deflection ratio of eq. 24 solely depends on the dimensionless terms ϕ and Θ, as, from eqs. 16, 12 and 13, it occurs that term λL_{4p} is also a function of these two terms:

$$\lambda L_{4p} = \lambda L = \frac{2}{\phi}\sqrt{\frac{1}{\Theta\left(\pi^2 - 6\right)}} \tag{25}$$

Finally, the total deflection of the culm during the four-point bending test $\delta_{tot,4p}$, when there is a longitudinal crack at the side of the culm, occurs as a function of the bending-moment-induced deflection $\delta_{b,4p}$ from eqs. 2, 5 and 24:

$$\delta_{tot,4p} = \delta_{b,4p} + \delta_{s,4p} + \delta_{t,4p} = \left\{ 1 + \frac{3}{c_{i,4p}}\Theta \cdot \left\{ \frac{1}{k_s} + 12\phi^2 \left[1 - \frac{2\sinh\left(\frac{\lambda L_{4p}}{2}\right)}{\lambda L_{4p}\left[2\cosh\left(\lambda L_{4p}\right) - 1\right]} \right] \right\} \right\} \delta_{b,4p} \tag{26}$$

where $c_{i,4p} = 23$.

4 Effect of friction at the load application points

Typical bending test setups for bamboo involve straps or wooden saddles at the supports and at the load application points (fig. 4a-c) [12, 15, 20, 27, 31], to distribute the load to as much of the culm circumference as possible. Alternatively, sometimes the load is applied via a flat surface (fig. 4d, e.g., a steel plate [20]). The analysis of Section 3 assumes a) that these supports can resist the applied torque, and, b)that the load application configuration does not provide any torsional restraint. This section examines the validity of these assumptions, with emphasis on how the friction that develops at the interface between the straps/saddles/plates and the culm, affects the torsion-induced deflections.

Regarding the first assumption, at the supports, the vertical reaction passes through the center of the cross-section, and therefore creates a torque about the shear center S, of the same magnitude and opposite direction, compared to the torque caused by load P at the load application points (fig. 4a). This, combined with the friction between the saddles and the culm, indicates that the supports can resist the applied torque. Regarding the second assumption, at the load application points, friction provides some torsional restraint, therefore the applied torque on the culm is less than the assumed $T_0 = 2PR$. In order to investigate this further, this section considers three commonly used load application configurations; the strap configuration of fig. 4b, the saddle configuration of fig. 4c [12], and the flat surface configuration of fig. 4d [20].

In the strap configuration, the distributed load q, normal to the culm surface, is $q = 2P/\pi \cdot \cos\omega$ (where ω is the angular coordinate along the culm circumference (fig. 4b), positive clockwise), applied on the top half of the culm ($-\pi/2 \leq \omega \leq \pi/2$). Hence, when the culm starts twisting, a distributed frictional load $f_s = \mu \cdot 2P/\pi \cdot \cos\omega$, that resists the motion, develops at the strap-culm interface (where μ is the friction coefficient of the interface). Frictional load f_s creates a total torque T_F about the shear center S, equal to:

$$T_F = \mu \frac{4PR_o}{\pi} \tag{27}$$

where R_o denotes the outer radius of the culm. Torque T_F acts in the direction opposite to T_0, therefore the torque T_1 that eventually loads the culm is:

$$T_1 = T_0 - T_F = 2PR\left(1 - \frac{R_o}{R}\frac{4\mu}{\pi}\right) \tag{28}$$

where R is the midline radius of the culm. Further taking into account that:

$$\frac{R_0}{R} = \frac{R + \frac{t}{2}}{R} = 1 + \frac{1}{2\phi} \tag{29}$$

T_1 occurs as a function of the culm shape factor ϕ:

$$T_1 = 2PR\left[1 - \left(1 + \frac{1}{2\phi}\right)\frac{4\mu}{\pi}\right] \tag{30}$$

Equation 30 shows that torque T_1 is less than T_0, by a factor r_0 equal to:

$$r_0 = \left(1 + \frac{1}{2\phi}\right)\frac{4\mu}{\pi} \tag{31}$$

which depends on the culm shape factor ϕ and the friction coefficient μ of the strap-culm interface (fig. 4b). The deflection due to torsion δ_t (eq. 17) also decreases by the same factor. Throughout this study, we refer to the newly-introduced factor r_0 as torque reduction factor.

As a different load application configuration case, consider the saddle configuration of fig. 4c. The reference saddle configuration involves a wooden saddle with a 90^o notch, which prevents lateral movement of the culm. When the culm starts twisting, frictional forces $F_s = \mu \cdot P/\left(2\cos\omega_1\right)$ at the contact points between the culm and the saddle resist the motion (where $\omega_1 = 45^o$, fig. 4c). In this case, the total torque T_F about shear center S is:

$$T_F = 2F_sR_o = \mu\frac{PR_o}{\cos\omega_1} \tag{32}$$

Therefore, the torque T_1 that eventually loads the culm is:

$$T_1 = 2PR\left[1 - \left(1 + \frac{1}{2\phi}\right)\frac{\mu}{2\cos\omega_1}\right] \tag{33}$$

and thus the torque reduction factor r_0 in the case of the saddle configuration is:

$$r_0 = \left(1 + \frac{1}{2\phi}\right)\frac{\mu}{2\cos\omega_1} \tag{34}$$

Thus, in the saddle case, r_0 additionally depends on the angle ω_1 of the saddle notch (besides shape factor ϕ and friction coefficient μ).

Further, in the case of the flat surface configuration (e.g. when the load is applied via a steel plate), there is only one contact point, where friction force F_s creates a torque $T_F = \mu PR_0$ about the shear center S (fig. 4d). Following the same procedure as in the previous cases, the torque reduction factor r_0 for the case of a load applied via a flat surface is:

$$r_0 = \left(1 + \frac{1}{2\phi}\right)\frac{\mu}{2} \tag{35}$$

Equation 34 coincides with eq. 35 when $\omega_1 \to 0$.

Equations 31, 34 and 35 indicate that the strap configuration is the most effective regarding torque mitigation. Additionally, since $\cos\omega_1 \leq 1$, the saddle configuration can mitigate the torsion-induced stiffness loss more effectively than the flat surface configuration (eqs. 34 and 35). This has important implications for full-culm bamboo structures, suggesting that the manner in which loads are transferred to the beams can mitigate stiffness loss when cracks appear. It also has ramifications for testing standards, indicating that the standards should specify the exact load application configuration for the test results to be consistent.

Figure 5 illustrates the effect of shape factor and friction coefficient on the torque reduction factor r_0. It shows that, for typical for bamboo values of the shape factor (ϕ=3∼6 [13]), and for typical values of μ for wood and wood products (μ=0.2∼0.4, e.g. [32, 33]), the torque reduction is significant (15%∼56%),

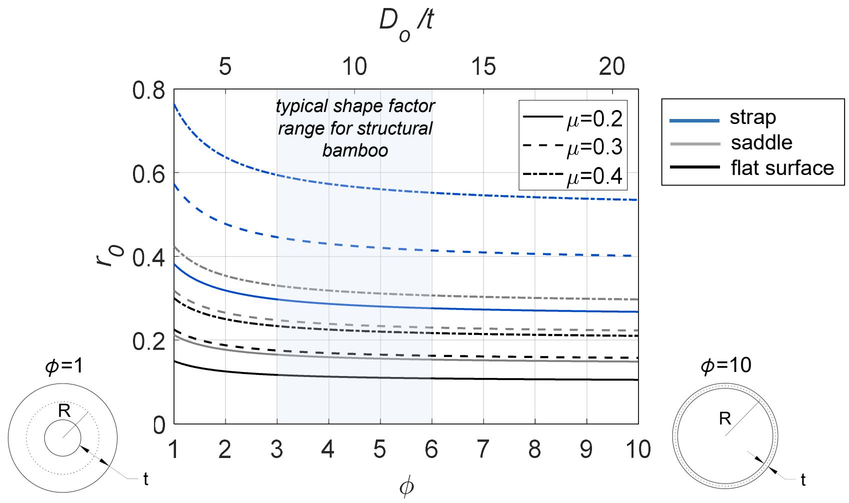

Fig. 5 Torque reduction factor versus culm shape factor $\phi = R/t$ and ratio of external diameter to thickness D_o/t for various friction coefficient values

especially in the strap configuration (28%∼56%). Figure 5 also shows that r_0 reduces with shape factor, but the effect is more prominent for low shape factor values (thick-walled sections). For $\phi > 4 \sim 5$, further increase of the shape factor has no significant effect on the torque reduction.

4.1 Effect of friction on stiffness loss

Since friction mitigates the torsional load applied on the culm, it follows that it mitigates proportionately torsion-induced deflections. Thus, taking into account torque reduction because of friction at the load application points, eqs. B6 (three-pont bending test) and 26 (four-point bending test) become:

$$\delta_{tot} = \left\{ 1 + \frac{3}{c_i} \Theta \cdot \left[\frac{1}{k_s} + 12\phi^2 C_i \left(1 - r_0\right) \right] \right\} \delta_b \tag{36}$$

where r_0 is the torque reduction factor (eqs. 34, 35), $c_{i,3p} = 8$, $c_{i,4p} = 23$, and

$$C_{i,3p} = 1 - \frac{\tanh\left(\lambda L_{3p}\right)}{\lambda L_{3p}} \tag{37}$$

$$C_{i,4p} = 1 - \frac{2\sinh\left(\frac{\lambda L_{4p}}{2}\right)}{\lambda L_{4p}\left[2\cosh\left(\lambda L_{4p}\right) - 1\right]} \tag{38}$$

Note that subscripts '3p' and '4p' denote the three-point and four-point bending tests respectively.

Subsequently, having specified shear- (δ_s) and torsion-induced deflections (δ_t) as a function of the moment-induced deflection (δ_b), the ratio of final (with crack, K_t) over initial (without crack, K_0) stiffness occurs from eqs. 5 and 36:

$$\frac{K_t}{K_0} = \frac{\delta_b + \delta_s}{\delta_{tot}} = \left(1 + \frac{3\Theta}{c_i k_{s,c}}\right) \Big/ \left\{ 1 + \frac{3}{c_i}\Theta \cdot \left[\frac{1}{k_{s,o}} + 12\phi^2 C_i \left(1 - r_0\right)\right]\right\} \tag{39}$$

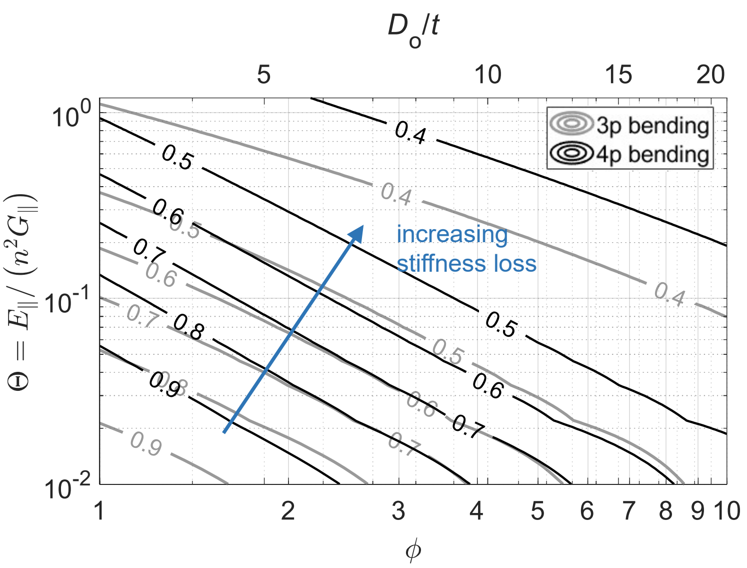

Fig. 6 Stiffness loss (final stiffness K_t over initial stiffness K_0) versus culm shape factor $\phi = R/t$ (or ratio of external diameter to thickness D_o/t) and shear-torsion deflection factor $\Theta = E_{\parallel}/(n^2 G_{\parallel})$ (eq. 39), ignoring the effect of friction.

where C_i as in eqs. 37 and 38 for the three-point and four-point bending test respectively. Note that C_i solely depends on the product λL (eq. 25), which is a function of the dimensionless terms ϕ (shape factor, eq. 22) and Θ (shear-torsion deflection factor, eq. 6). Equation 39 takes into account shear deformations before and after the crack occurs; $k_{s,c} = 0.5$ is the shear correction factor of a closed section, and $k_{s,o} = 0.17$ is the shear correction factor of a thin-walled open section. Equation 39 indicates that the stiffness loss, when a crack opens at the side of the culm, depends on three dimensionless parameters; i.e., shear-torsion deflection factor Θ, culm shape factor ϕ, and torque reduction factor r_0. The latter, besides shape factor ϕ, depends on friction coefficient between the culm and the surface that transfers the load to the culm (eqs. 34, 35) and the shape of that surface (fig. 4).

Figure 6 illustrates the effect of shape factor ϕ and shear-torsion deflection factor Θ on ratio K_t/K_0 (eq. 39), ignoring the mitigating effect of friction. It shows that stiffness loss increases with increasing ϕ and Θ. Thus, thin-walled sections (large values of ϕ), and low shear modulus $G_{\parallel}$ or short shear span lengths (large values of Θ) lead to more prominent stiffness loss.

To quantify stiffness loss, we adopt indicative values of geometrical and material properties; e.g., $E_{\parallel}/G_{\parallel}$=6.5, n=12 ($\Theta = 0.045$). Figure 7 illustrates stiffness loss (eq. 39) as a function of shape factor ϕ, for no torque reduction (r_0=0) and for a torque reduction factor r_0=20%. Figure 7 shows that, for the same shear span, stiffness loss is higher in the three-point bending test compared to the four-point bending test. Additionally, it shows that a representative value of torque reduction factor r_0=20% leads to a mitigation of stiffness loss of approximately 5% K_0, compared to not considering friction at the load application points.

As an example, assume a representative for Moso bamboo value of the shape factor, i.e., ϕ=5. The thus occurring stiffness reduction (1-K_t/K_0), assuming a torque reduction due to friction r_0=20%, is 48% for the three-point bending test and 41% for the four-point bending test. The corresponding values without taking friction into account (thus, r_0=0) are 54% for the three-point bending test and 46% for the four-point bending test. Note however that the stiffness loss is that significant only when the crack extends at almost

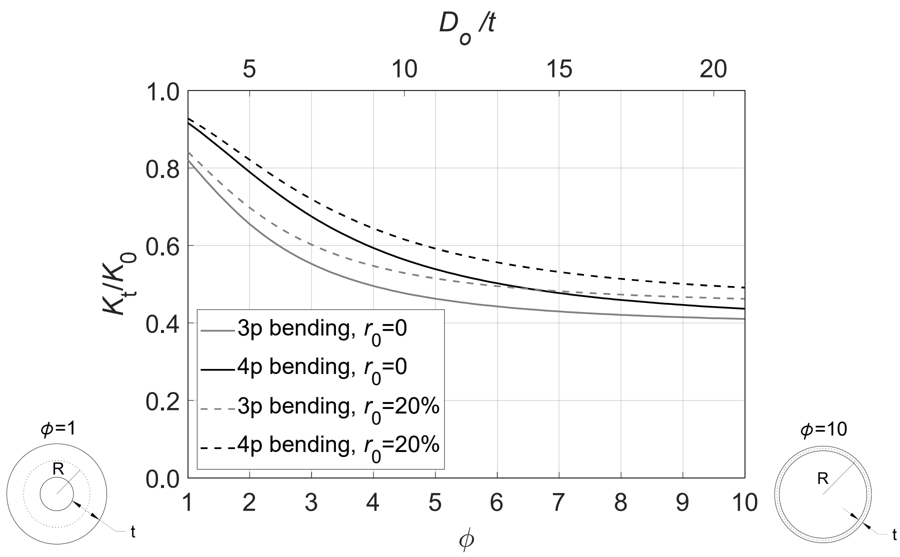

Fig. 7 Stiffness loss (final stiffness K_t over initial stiffness K_0) versus culm shape factor $\phi = R/t$ and ratio of external diameter to thickness D_o/t for $\Theta = E_{\parallel}/(n^2 G_{\parallel}) = 0.045$.

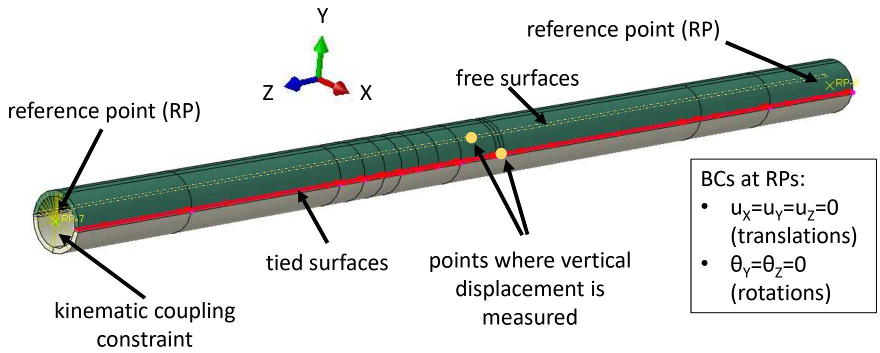

Fig. 8 Numerical model assignments.

the entire span length. This is because the torsional constant of the closed section is $J_{s,c} = 2\pi R^3 t$, which makes it $3\phi^2$ times higher than the torsional constant of the open section ($J_{s,o} = \frac{2}{3}\pi R t^3$). For a typical shape factor value (i.e., $\phi = 5$), this translates to a torsional rigidity ($G_{\parallel} J_s$) of the closed section being 75 times higher than that of the open section. Hence, the resulting torsion-related deflections are considerably smaller, if the crack is not present along the entire span.

5 Comparison with numerical results

The previous sections derive analytical expressions that describe the mixed flexural-torsion problem that occurs when an open-section tube is subjected to three- or four-point bending. To verify the proposed equations, this section develops numerical models of a three- and a four-point bending test in the commercial finite element software Abaqus [34]. The shear span length is L=1000 mm for both tests, therefore total span length is 2000 mm for the three-point and 3000 mm for the four-point bending test. The analysis utilizes the dynamic implicit solver, which employs the HHT-α integration scheme, with α=0.33. Both models simulate the bamboo culm as an idealized cylinder, of external radius R_o=99 mm and thickness t=9 mm (shape factor ϕ=5). To simulate the longitudinal crack, the idealized cylinder comprises two half-cylinders,

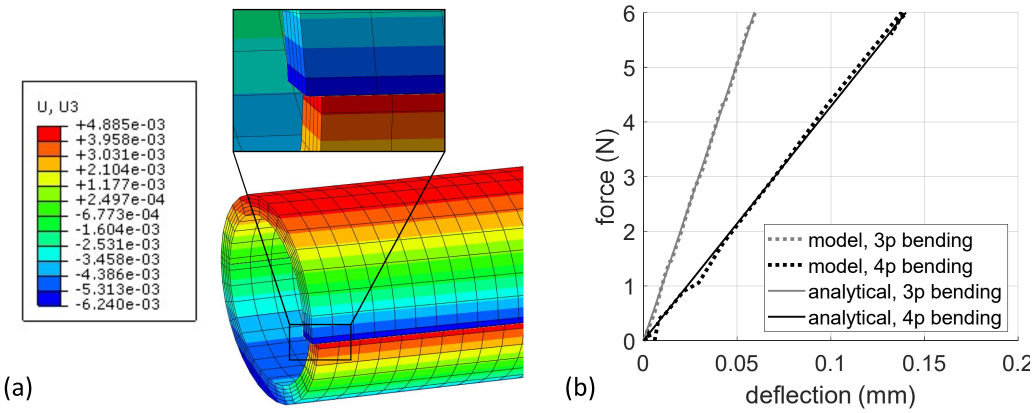

Fig. 9 a) Warping displacement at the support, and b) comparison between numerical and analytical force-displacement curves for a culm with a longitudinal crack at the side.

tied together on one side, while on the other side there is not interaction between the half-cylinder surfaces (fig. 8). The mesh consists of 3D-solid, 8-node linear elements (C3D8, 24 degrees of freedom per element), and mesh size is 10 mm. The material is elastic and isotropic, with Young's modulus $E = E_{\|}$=12500 MPa and Poisson's ratio ν=0.3. The isotropic material assumption is not accurate for bamboo, but the approximation is sufficient to verify the proposed equations. This is because a) only material properties in the longitudinal direction come into the equations, and b) this study examines global response and not local phenomena (e.g., stress distribution under point loads) [35]. Load is applied on the culm as a uniform traction that follows surface rotation, acting on an area of approximately 20 mm x 20 mm. Regarding boundary conditions at the supports, to achieve the assumed free warping but no twisting, and to ensure simultaneously a pinned support for flexure, the model involves, at each support, a reference point at the center of the cross-section, and a kinematic coupling constraint of the reference point with the cross-section surface (fig. 8). The reference points are free to rotate in the direction of the bending moment, but the rest of the degrees of freedom (translations and rotations) are restrained.

Figure 9 shows the model force-displacement curves for the three-point and four-point bending tests, and the corresponding force-displacement curves from eqs. B6 and 26. For the model curves, the load is the sum of the vertical loads at the reference points, and the deflection is the average vertical displacement of two points, defined by the horizontal plane that contains the neutral axis and the outer surface of the culm, at the cross-section of the midspan (fig. 8). Considering the average displacement of these two points is necessary, to eliminate vertical displacements associated with twisting of the cross-section. The numerical and analytical results are in agreement, which verifies the applicability of the proposed equations.

6 Comparison with experimental results

To verify that the analytical expressions apply to actual bending tests, this section compares the predictions of the present analysis with the experimental results of [20]. That study [20] initially determined the modulus of elasticity of six Moso bamboo culms (*Phyllostachys edulis*), via three-point bending tests (performed in the elastic stage). Subsequently, it tested the specimens again, after creating a longitudinal crack at their

Table 1 Three-point bending specimen properties [20] and corrected Young's modulus $E_{\parallel}$

specimen no	E_{app} (MPa)	external diameter D (mm)	thickness t (mm)	corrected $E_{\parallel}$ (MPa)	experimental K_t/K_0
1	11190	72.4	7.4	12437	0.54
2	10057	72.2	7.2	11053	0.59
3	11945	71.6	7.3	13342	0.46
4	14696	69.3	8.2	16630	0.38
5	13000	77.3	8.2	14970	0.36
6	16218	70.5	6.8	18848	0.43

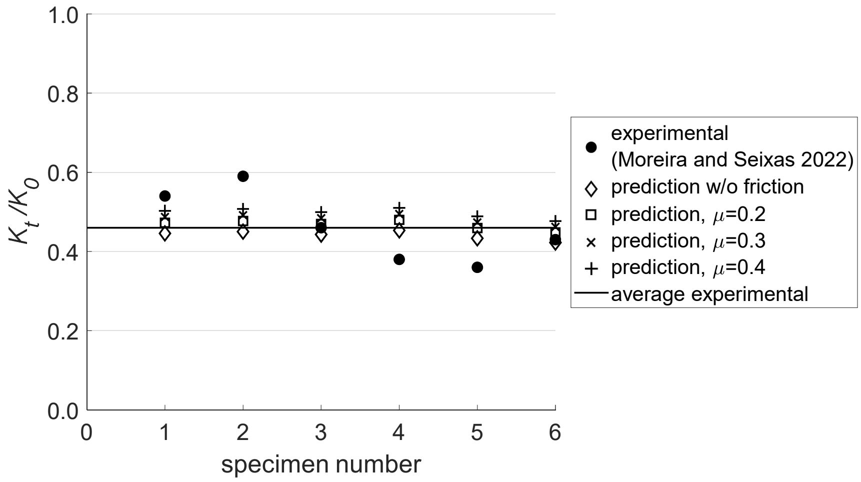

Fig. 10 Comparison between analytically predicted loss of stiffness and experimental results [20] for a culm with a longitudinal crack at the side.

side, to determine the stiffness loss because of the crack. Total span length of the tests was 1000 mm (shear span length 500 mm), specimen properties as in Table 1, and test setup for the load application was the flat surface configuration.

To adopt eq. 39, and since shear deflections are significant (Section 2), initially we correct the experimental values of the modulus of elasticity [20] for shear. Let E_{app} be the experimental value of the modulus of elasticity of the intact culms, calculated from the slope of the force-displacement curve (without consideration for shear). For the total deflection δ at the midspan, it holds that:

$$\delta = \frac{PL_{3p}^3}{6E_{app}I} = \frac{PL_{3p}^3}{6E_{\parallel}I} + \frac{PL_{3p}}{2k_{s,c}G_{\parallel}A} \tag{40}$$

where $k_{s,c}$=0.5 the shear correction factor of the closed section. Therefore, substituting $L_{3p} = 2nR$, $I/A = R^2/2$, and rearranging, the corrected for shear Young's modulus parallel to the fibers $E_{\parallel}$ occurs:

$$E_{\parallel} = E_{app}\left(1 - \frac{3E_{app}}{8k_{s,c}n^2G_{\parallel}}\right)^{-1} \tag{41}$$

Table 1 shows the corrected according to eq. 41 values for $E_{\parallel}$.

Figure 10 compares the experimental results of K_t/K_0 [20] with the results of eq. 39, for various values of the friction coefficient μ, adopting the flat surface load application configuration in the reduction factor calculations. Table 1 shows the parameters used for the analytical calculations of fig. 10. Figure 10 indicates that eq. 39 accurately predicts the average experimental stiffness loss, although the analytical prediction does not reflect the scatter of the experimental results.

7 Discussion and conclusions

Longitudinal splitting of full-culm bamboo structural members is highly probable during the lifetime of a bamboo structure. The uncertainties associated with incomplete understanding of the behavior of slit bamboo structural members induce ambiguities in the engineering design of those members, thus posing a potential threat to the safety of existing and future full-culm bamboo structures. The present study investigates the stiffness loss occurring in full-culm bamboo flexural members, after they obtain a longitudinal crack extending throughout the entire span length. The analysis assumes that the crack is present along the entire span length, and therefore it is a lower-bound approach for the stiffness calculations. The study develops analytical expressions that describe the stiffness loss, assuming tubular culm geometry of constant diameter and thickness, and verifies them with numerical simulations and available experimental results. All the calculations assume thin-walled sections for simplicity, and thus their accuracy is expected to be reduced for thick-walled section cases. Moreover, the calculations ignore the (imperfect) warping restraint the nodes provide, and thus they yield conservative deflection values Nevertheless, the predictions of this study are in reasonable agreement with available experimental results, which indicates that the effect of nodes is probably not significant.

The study examines two load cases; three-point flexure and four-point flexure, and compares the stiffness of a slit culm to that of an intact culm. It indicates that the stiffness loss is mainly due to the torsional effects, which occur because of the eccentric position of the shear center of the open tubular section. Secondary cause is the larger contribution of shear deformations in the case of the open section compared to the closed section. Notably, stiffness loss solely depends on two dimensionless parameters; i.e., culm shape factor (radius-to-thickness ratio), and the herein introduced shear-torsion deflection factor, which is a function of material properties (Young's modulus parallel to the fibers and shear modulus parallel to the fibers), and ratio of shear span length to culm diameter. Moreover, the study proves analytically that the friction at the load application surface has a mitigating effect on the torque applied on the culm, and thus on torsion-induced deflections. This is important for full-culm bamboo structures, suggesting that the manner in which the load is transferred to the beams can mitigate splitting-induced stiffness loss.

The present study also indicates that shear deformations are significant in the three-point bending test, and in the cracked-section four-point bending test, and cannot be ignored for typical bamboo material properties. On the contrary, in the intact-section four-point bending test, shear deformations are negligible for common shear span lengths (larger than approximately 8 times the culm diameter). Thus, for typical values of bamboo material and geometrical properties, shear- and torsion-induced deflections result in substantial stiffness loss (40%∼50%) when a crack appears (compared to the initial stiffness of an intact culm), both for the three-point and the four-point bending test. These values assume common shear span lengths (approximately 10 times the culm diameter) and include the mitigating effect of friction at the load application points. Not taking friction into account would lead to an additional 5%∼6% stiffness loss. Moreover, for the same shear span length, the stiffness loss is approximately 8% larger in the three-point bending test compared to the four-point bending test. These estimations assume however that the crack extends on the entire span length. If the crack is not sufficiently large, torsional effects do not affect the stiffness significantly. This is because the torsional rigidity of the intact section is 75 times higher than that of the open section, thus rendering torsion-induced deflections negligible.

In practice, the results of this study indicate that the design stiffness of bamboo flexural members should be the cracked stiffness, and not the intact culm stiffness, similarly to concrete structures. The actual cracked stiffness is not easy to calculate, as it depends on the number and position of the cracks, and, when torsional effects occur, on the load application conditions (friction and manner in which the load is applied on the culms). In this context, a single crack at the culm side, that extends throughout the entire span length, is an extreme case, and not likely to occur in practical applications. This means that the herein produced results, which indicate a stiffness loss of 40%-50%, are lower-bound results. In general, we would suggest the adoption of the cracked stiffness in the design of full-culm bamboo structural members, or, alternatively, the use of confinement to restore continuity, and thus mitigate stiffness loss.

Overall, this study provides analytical tools for the estimation of stiffness loss after a longitudinal crack appears on a bamboo culm subjected to flexure. The present analysis has important ramifications for testing standards, as it indicates that the load application configuration can affect the test results. Additionally, since cracks are common in bamboo flexural members, this study is an important step towards rational engineering design of full-culm bamboo structures.

Acknowledgements

The authors thank Dr. Nischal Pradhan for providing the bamboo bending test photos of fig. 1. This work was supported by the University Grants Committee Research Grants Council of Hong Kong, under Grant Reference Number GRF 16213321.

Appendix A Schematic representation of the torsion problem

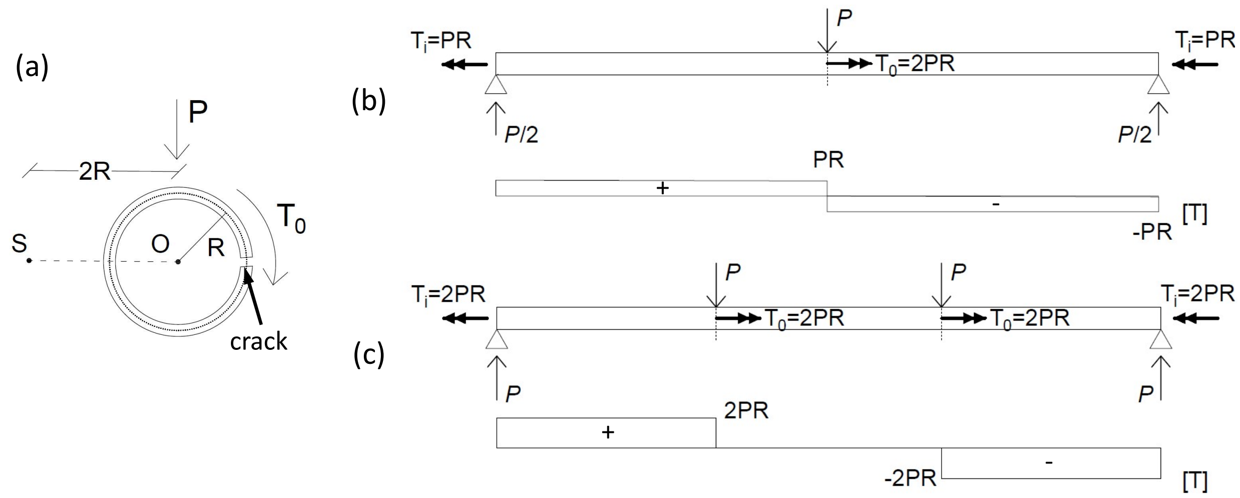

Fig. A1 Open cross-section and shear center (a), and total torque diagrams for the three-point (b) and four-point (c) bending test.

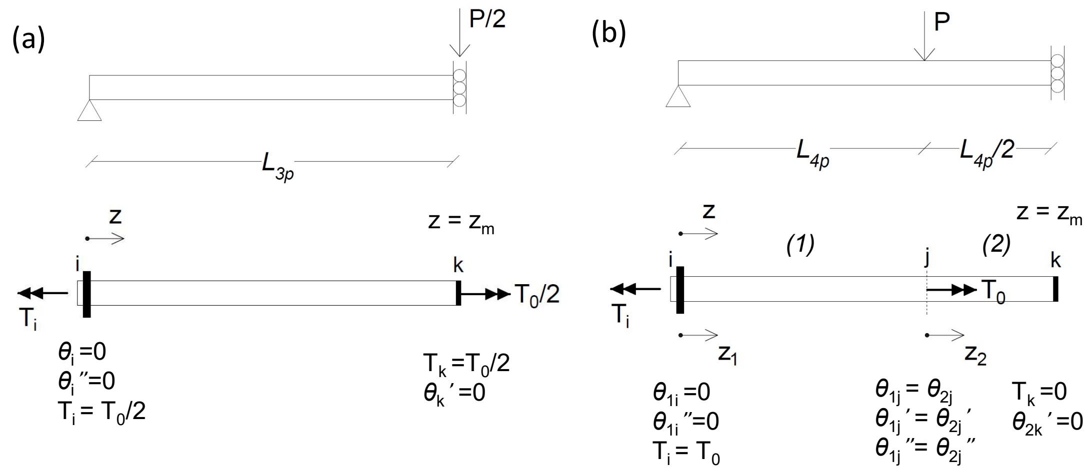

Fig. A2 Boundary conditions to solve the mixed torsion and warping problem for (a) the three-point and (b) the four-point bending test.

Appendix B Torsion in the three-point bending test

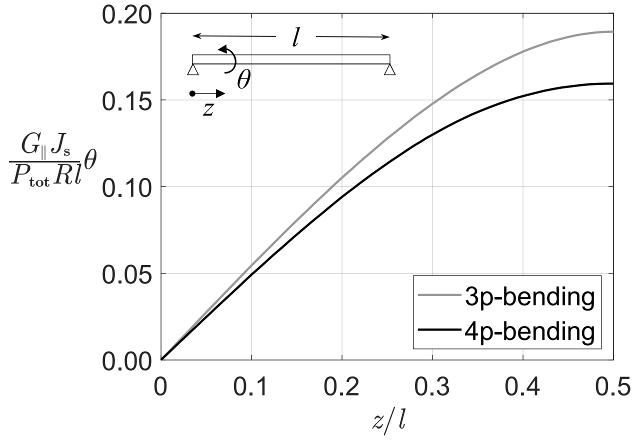

Fig. B3 Normalized angle of twist θ along the beam for the three-point and four-point bending test (P_{tot} is the total load for each test and l is the total span length). The plot assumes the same span length for both tests (normalized shear span length $n_{3p} = 1.5n_{4p} = 10$), $E_{\|}/G_{\|} = 4.5$ and shape factor ϕ=5 (eq. 22).

In the three-point bending test, and considering half of the beam because of symmetry, the load at end k (fig. A2a) is $P/2$. The torque acting at the end k, because of the load is $T_0 = 0.5P \cdot 2R = PR$ (fig. A2a). Applying the boundary conditions, the resulting solution for angle of twist θ_{3p} is (fig. B3):

$$E_{\|} J_w \theta_{3p}(z) = \frac{PR}{\lambda^2}\left[z - \frac{\sinh(\lambda z)}{\lambda \cosh(\lambda L_{3p})}\right] \tag{B1}$$

where $0 \leq z \leq L_{3p}$ (fig. A2a). Figure B3 shows that the angle of twist in the three-point bending test is larger than in the three-point bending test, assuming the same total load and total span length. The expressions for Saint-Venant torque $T_{s,3p}$ and warping bimoment $B_{w,3p}$ ensue by substituting eq. B1 into eqs. 10 and 11:

$$T_{s,3p}(z) = PR\left[1 - \frac{\cosh(\lambda z)}{\cosh(\lambda L_{3p})}\right] \tag{B2}$$

$$B_{w,3p}(z) = -PR\frac{\sinh(\lambda z)}{\lambda \cosh(\lambda L_{3p})} \tag{B3}$$

where P is the load at the middle of the culm and L_{3p} is the shear span length of the three-point bending test, equal to half the total span. Note that, although the applied boundary conditions assume that the culm does not twist at the supports, eqs. B2 and B3 are valid regardless, as long as the rest of the boundary conditions remain the same. Whether the culm twists at the supports or not, only affects the resulting angle of twist θ (eq. B1).

Subsequently, the deflection due to torsion for the three-point bending test ($\delta_{t,3p}$) occurs by substituting eqs. B2 and B3, into eq. 17, taking into account eqs. 12 and 13, and calculating the integrals for $z_m = L_{3p}$. $\overline{T}_s$ and $\overline{B}_w$ in eq. 17 (Saint-Venant torque and warping bimoment, because of the virtual load) occur by setting P=1 in eqs. B2, B3. Thus:

$$\delta_{t,3p} = \frac{6Pn\phi^3}{\pi G_{\parallel} R} \cdot \left[1 - \frac{\tanh\left(\lambda L_{3p}\right)}{\lambda L_{3p}}\right] \tag{B4}$$

where ϕ is the dimensionless shape factor of the culm (eq. 22) and n is the dimensionless shear span length ($n = L_{3p}/\left(2R\right)$). Subsequently, combining eq. B4 with eq. 1:

$$\frac{\delta_{t,3p}}{\delta_{b,3p}} = \frac{9}{2}\Theta\phi^2 \left[1 - \frac{\tanh\left(\lambda L_{3p}\right)}{\lambda L_{3p}}\right] \tag{B5}$$

where Θ is the shear-torsion deflection factor, as in eq. 6. The deflection ratio of eq. B5 solely depends on the dimensionless terms ϕ and Θ (see also eq. 25). Finally, the total deflection of the culm $\delta_{tot,3p}$, during the three-point bending test, when there is a longitudinal crack at the side of the culm, occurs as a function of the deflection due to the bending moment $\delta_{b,3p}$ from eqs. 1, 5 and B5:

$$\delta_{tot,3p} = \delta_{b,3p} + \delta_{s,3p} + \delta_{t,3p} = \left\{1 + \frac{3}{c_{i,3p}}\Theta \cdot \left\{\frac{1}{k_s} + 12\phi^2 \left[1 - \frac{\tanh\left(\lambda L_{3p}\right)}{\lambda L_{3p}}\right]\right\}\right\} \delta_{b,3p} \tag{B6}$$

where $c_{i,3p} = 8$.

References

[1] Janssen, J.A.A.: Bamboo in building structures. PhD thesis, University of Eindhoven (1981)

[2] Liese, W.: Research on bamboo. Wood Sci. Technol. **21**(3), 189–209 (1987)

[3] Amada, S., Ichikawa, Y., Munekata, T., Nagase, Y., Shimizu, H.: Fiber texture and mechanical graded structure of bamboo. Compos. B. Eng **28**(1), 13–20 (1997). https://doi.org/10.1016/S1359-8368(96)00020-0. Use of Composites Multi-Phased and Functionally Graded Materials

[4] Wu, W., Liu, Q., Zhu, Z., Shen, Y.: Managing bamboo for carbon sequestration, bamboo stem and bamboo shoots. Small-Scale For **14**(2), 233–243 (2015). https://doi.org/10.1007/s11842-014-9284-4

[5] Huang, L., Krigsvoll, G., Johansen, F., Liu, Y., Zhang, X.: Carbon emission of global construction sector. Renew. Sustain. Energy Rev **81**, 1906–1916 (2018). https://doi.org/10.1016/j.rser.2017.06.001

[6] ISO 22156:2021(E): Bamboo structures - Bamboo culms -Structural design. International Organization for Standardization (2021)

[7] Wang, X., Ren, H., Zhang, B., Fei, B., Burgert, I.: Cell wall structure and formation of maturing fibres of moso bamboo (*Phyllostachys pubescens*) increase buckling resistance. J R Soc Interface **9**(70), 988–996 (2012). https://doi.org/10.1098/rsif.2011.0462

[8] Dixon, P.G., Gibson, L.J.: The structure and mechanics of Moso bamboo material. J R Soc Interface **11**(99), 20140321 (2014). https://doi.org/10.1098/rsif.2014.0321

[9] Wang, Y., Zhang, C., Chen, W.: An analytical model to predict material gradient and anisotropy in bamboo. Acta Mech. **228**(8), 2819–2833 (2017). https://doi.org/10.1007/s00707-015-1514-0

[10] Sharma, B., Harries, K.A., Ghavami, K.: Methods of determining transverse mechanical properties of full-culm bamboo. Constr Build Mater. **38**, 627–637 (2013). https://doi.org/10.1016/j.conbuildmat.2012.07.116. 25th Anniversary Session for ACI 228 – Building on the Past for the Future of NDT of Concrete

[11] Richard, M.J., Gottron, J., Harries, K.A., Ghavami, K.: Experimental evaluation of longitudinal splitting of bamboo flexural components. Proceedings of the Institution of Civil Engineers - Structures and Buildings **170**(4), 265–274 (2017). https://doi.org/10.1680/jstbu.16.00072

[12] Lorenzo, R., Mimendi, L., Yang, D., Li, H., Mouka, T., Dimitrakopoulos, E.G.: Non-linear behaviour and failure mechanism of bamboo poles in bending. Constr Build Mater. **305**, 124747 (2021). https://doi.org/10.1016/j.conbuildmat.2021.124747

[13] Mouka, T., Dimitrakopoulos, E.G., Lorenzo, R.: Insight into the behaviour of bamboo culms subjected to bending. J. R. Soc. Interface (*in press*). https://doi.org/10.1098/rsif.2021.0913

[14] Wegst, U.G.K.: Bamboo and wood in musical instruments. Annu. Rev. Mater. Res. **38**(1), 323–349 (2008). https://doi.org/10.1146/annurev.matsci.38.060407.132459

[15] Trujillo, D., Jangra, S., Gibson, J.M.: Flexural properties as a basis for bamboo strength grading. Proc. Inst. Civ. Eng.: Struct. Build. **170**(4), 284–294 (2017). https://doi.org/10.1680/jstbu.16.00084

[16] Amada, S., Untao, S.: Fracture properties of bamboo. Compos. B. Eng **32**(5), 451–459 (2001). https://doi.org/10.1016/S1359-8368(01)00022-1

[17] Shao, Z.-P., Fang, C.-H., Tian, G.-L.: Mode I interlaminar fracture property of moso bamboo (*Phyllostachys pubescens*). Wood Sci. Technol. **43**, 527–536 (2009). https://doi.org/10.1007/s00226-009-0265-2

[18] Mitch, D., Harries, K.A., Sharma, B.: Characterization of splitting behavior of bamboo culms. J. Mater. Civ. Eng. **22**(11), 1195–1199 (2010). https://doi.org/10.1061/(ASCE)MT.1943-5533.0000120

[19] Mannan, S., Parameswaran, V., Basu, S.: Stiffness and toughness gradation of bamboo from a damage tolerance perspective. Int J Solids Struct **143**, 274–286 (2018). https://doi.org/10.1016/j.ijsolstr.2018.03.018

[20] Eustáquio Moreira, L., Seixas, M.: Analysis of the bending behavior of bamboo culms with a full longitudinal crack. Eng Struct **251**, 113501 (2022). https://doi.org/10.1016/j.engstruct.2021.113501

[21] Timoshenko, S., Gere, J.M.: Theory of Elastic Stability 2e. McGraw-Hill, New York (1970)

[22] Vlasov, V.Z.: Thin-walled Elastic Beams, 2nd Ed. Rev. and Augm. Translated from Russian [by Y. Schectman]. Israel Program for Scientific Translations, Jerusalem (1961)

[23] Cook, R.D., Young, W.C.: Advanced Mechanics of Materials, 2nd edn. Prentice-Hall Inc., Upper Saddle River, New Jersey 07458, US (1999)

[24] Liu, J., Cheng, S.: Analysis of orthotropic beams. US Dep. of Agriculture, Forest Products Laboratory (FPL 343) (1979)

[25] Savoia, M., Tullini, N.: Beam theory for strongly orthotropic materials. Int. J. Solids Struct. **33**(17), 2459–2484 (1996). https://doi.org/10.1016/0020-7683(95)00163-8

[26] ISO 22157:2019(E): Bamboo Structures - Determination of physical and mechanical properties of bamboo culms- Test methods. International Organization for Standardization (2019)

[27] Nurmadina, Nugroho, N., Bahtiar, E.T.: Structural grading of gigantochloa apus bamboo based on its flexural properties. Constr Build Mater. **157**, 1173–1189 (2017). https://doi.org/10.1016/j.conbuildmat.2017.09.170

[28] Freund, J., Karakoç, A.: Shear and torsion correction factors for Timoshenko beam theory. Res. Eng. Struct. Mater. **2**, 19–27 (2016). https://doi.org/10.17515/resm2015.19me0827

[29] Gauss, C., Savastano, H., Harries, K.A.: Use of ISO 22157 mechanical test methods and the characterisation of brazilian *P. edulis* bamboo. Constr Build Mater. **228**, 116728 (2019). https://doi.org/10.1016/j.conbuildmat.2019.116728

[30] Tarn, J.-Q., Chang, H.-H.: Torsion of cylindrically orthotropic elastic circular bars with radial inhomogeneity: some exact solutions and end effects. Int. J. Solids Struct. **45**(1), 303–319 (2008). https://doi.org/10.1016/j.ijsolstr.2007.08.012

[31] Sá Ribeiro, R.A., Sá Ribeiro, M.G., Miranda, I.P.A.: Bending strength and nondestructive evaluation of structural bamboo. Constr Build Mater. **146**, 38–42 (2017). https://doi.org/10.1016/j.conbuildmat.2017.04.074

[32] Bejo, L., Lang, E.M., Fodor, T.: Friction coefficients of wood-based structural composites. For. Prod. J. **50**(3), 39–43 (2000)

[33] Aira, J.-R., Arriaga, F., Íñiguez-González, G., Crespo, J.: Static and kinetic friction coefficients of

Scots pine (Pinus sylvestris L.), parallel and perpendicular to grain direction. Mater Construcc **64**, 030 (2014). https://doi.org/10.3989/mc.2014.03913

[34] Dassault Systémes: Simulia Abaqus V. 6.14-1, Vélizy-Villacoublay, France. https://www.3ds.com/products-services/simulia/products/abaqus/

[35] Silva, E.C.N., Walters, M.C., Paulino, G.H.: Modeling bamboo as a functionally graded material: lessons for the analysis of affordable materials. J. Mater. Sci. **41**, 6991–7004 (2006). https://doi.org/10.1007/s10853-006-0232-3